Brodogradnja/Shipbuilding/Open access
Volume 71 Number 1, 2020

Fatemeh Roshan
Abbas Dashtimanesh
Rasul Niazmand Bilandi

http://dx.doi.org/10.21278/brod71102

ISSN 0007-215X
eISSN 1845-5859

HYDRODYNAMIC CHARACTERISTICS OF TUNNELED PLANING HULLS IN CALM WATER

UDC 629.5.015.2:629.5.022
Original scientific paper

Summary

Tunneled planing hull is a special design of high-speed craft, which can reduce the frictional resistance to achieve higher velocities in high speeds. But, at lower speeds tunnels may lead to increase hull resistance. Therefore, tunneled planing hull design is an important issue which should be conducted with full prior information. In this study, a tunneled planing hull has numerically been studied in details using Star-CCM+ software. These simulations are based on Finite Volume Method (FVM) solution of Reynolds Averaged Navier-Stokes Equations (RANSE). Also, Volume of Fluid (VOF) method has been employed to obtain free surface variations, accurately. Morphing mesh approach has also been implemented to be able to simulate tunneled planing hull in two degrees of freedom in heave and pitch directions. Presented numerical setup has been validated by comparison of computed trim angle and hull resistant against the experimental results which have been presented by previous researchers. Afterwards, various physical phenomena around the considered tunneled planing hull as well as different physical parameters such as skin friction distribution, details of wetted surface area (total wetted surface, tunnel wetted surface, spray angle, keel and chain wetted length), shear and pressure drag, pressure distribution, wake pattern, and stream lines have been discussed, thoroughly. In this paper a new parameter as tunneled efficiency has been introduced based on obtained results. Tunnel efficiency shows appropriate speed range of planing hulls for using tunnel advantages in drag reduction. Presented results help designers to find new insight about the hydrodynamics of tunneled planing hulls.

Key words: *Tunneled hull; Planing craft; Numerical simulation; Hydrodynamic; Calm water*

1. Introduction

Boat designers always try to develop various complicated hull forms which can be used in racing boat competitions or luxury marine industries. In this regard, different kinds of planing hulls have been developed, so far. For example, stepped hulls are one of the designs which has been utilized in different marine areas. Stepped hulls have one or several transverse discontinuities in their bottom which lead to flow separation and drag reduction. Tunnel boats are another design which has been developed in naval industries. Creating tunnel in each side

of a planing hull leads to wetted surface reduction and aerodynamic lift generation. Hydrodynamic of this kind of hull is very complex. However, there are only few researches that have studied physics of tunneled boats.

Earlier, propeller tunnels were added to planing hull bottom to reduce the hull draft and propeller noise, and provide more flexibility in propeller and shaft placement [1]. The effects of propeller tunnel on hydrodynamic behavior of a planing hull have been studied by several researchers such as Millward[2], and Subramanian et al. [3]. Afterward, different tunnel configurations have been developed over the whole length of the hull to improve the boat performance.

Generally, a tunneled planing hull is a combined design of high speed planing hulls and high-speed multihulls. It can achieve to higher velocities by using the advantages related to both planing monohull and multihull craft. In this hull form, in addition to hydrodynamic lift, air flow can enter to the tunnels and produces the aerodynamic force over the hull surface. Since the aerodynamic drag is less than hydrodynamic drag, tunnel configuration leads to frictional resistance reduction in comparison with common planing hulls.

In this regard, Campbel [4] designed a tunneled hull to improve the stability, weight carrying ability and seakeeping capability of planing boats. He stated that developed tunneled hull always has positive trim angle and very high total lift, because of aerodynamic lift generation in the tunnels. It is interesting that although tunneled planing hulls have a small draft but their excellent longitudinal stability has been justified by Zou et al. [5].Small draft due to large total lift acting on the hull also leads to resistance reduction as mentioned before. Therefore, some researchers have also studied tunneled hull resistance characteristics in details, such as SU et al. [6, 7]. They measured and computed the resistance of series of tunneled planing hulls in different displacements and center of gravity locations. Yusefi et al. [8] arranged two tunnels in a planing monohull and compared resistance and trim angle against the original hull. They found that tunneled configuration can reduce the resistance by 14% relatives to primitive hull, in 50 Knot speed. Ghassabzadeh and Ghassemi [9] and Jiang et al. [10] also showed that resistance of tunneled hulls is significantly less than resistance of corresponding monohulls. They found that tunnel geometry has significant effect on resistance reduction. Therefore, Kazemimoghadam et al. [11] worked on resistance reduction in high speed tunneled planing hulls by considering five case studies with five different tunnel sizes. They showed that, reducing the tunnel aperture size can lead to resistance reduction because the air current dominates in the tunnels by using this method. Kazemimoghadam and Shafaghat [12] also presented the effects of tunnel height on drag reduction. Despite to these studies, hydrodynamic characteristics of tunneled planing hull have not been understood, completely and there is an urgent demand from industries to study the details of hydrodynamic phenomena related to tunneled planing hulls.

In this way, numerical methods are non-expensive and efficient technique to study the hydrodynamic characteristics of high speed planing hulls in details. Therefore, researchers have utilized various numerical softwares to predict planing hull behaviors and understand the details of fluid flow around the hull which cannot easily be captured by experimental facilities. For example, Ghadimi et al. [13] used a numerical method based on Reynolds average Navier Stokes (RANS) equations to simulate a planing hull in calm water. They were able to measure the trim angle, sinkage and hull resistance. One of most recent research in this area is related to Dashtimanesh et al. [14] that they have implemented StarCCM+ to study hydrodynamics of stepped planing hulls in calm water. They have calculated trim angle and resistance with a very good accuracy in comparison to experimental data. Numerical methods have also been used by Bilandi et al. [15] to predict wetted surface of stepped planing hulls.

Dicaterino et al. [16] and have also worked on planing hulls. They have used the numerical methods to predict planing hull performance. Dashtimanesh et al. [17] and Ghadimi et al [18] have simplified hydrodynamic prediction of a planing hull by using numerical simulation of planing flat plate in calm water. Moreover, some of tunneled planing hull studies have been done by numerical methods. Subramanyam et al. [19] computed the tunneled hull resistance and trim angle by using numerical method, and compared the obtained results against the same planing hull without the tunnels. They could present the pressure contours in tunnels and hull surface. Jiang et al. [20] used the both of experimental and numerical methods to predict the hydrodynamic characteristics of a tunneled planing hull. They could predict the trim angle, sinkage and resistance by good accuracy. However, in above mentioned researches, some of hydrodynamic characteristics, such as shear and pressure drag contributions in total drag, keel and chain wetted length, spray angle and tunnel wetted area, skin friction in quantitative and qualitative, stream lines, wake length and height behind the center line and tunnel and also hydrodynamic pressure in the tunnel have not been captured. Sheer and pressure drag contribution, skin frication distribution and wetted surface details, help designers to employed another method to reduce hull resistance and wetted surface.

Therefore, in this paper, the details of hydrodynamic behavior of a tunneled planning hull have been analyzed in details and appropriate design speed range for using tunnel configuration in hull have been introduced, numerically. Simulations have been performed in two degrees of freedom in pitch and heave directions. Obtained results have been validated against previous experimental measurement, which have been given by Ma et al. [21]. Subsequently, various hydrodynamic characteristics such as shear and pressure drag, water volume fraction, wetted surface area, keel and chine wetted length, spray angle, tunnel ventilation, stream line around the hull, wake profile, pressure distributions around the hull and in the tunnel, wake profile and lift percentage of tunnel. Also, a new parameter as tunnel efficiency have been introduced which have a useful role to predict appropriate design speed range for using tunneled planing hulls. Outside of this range, using tunnel may lead to increase hull resistance.

2. Governing Equations

Continuity and momentum equations govern the fluid flow phenomena. In marine hydrodynamics, it is assumed that the viscous fluid flow is incompressible and generally, Navier-Stokes equations can be written as follow:

$$\frac{\partial \bar{U}_i}{\partial x_i} = 0, \tag{1}$$

$$\frac{\partial \bar{U}_i}{\partial t} + \bar{U}_j \frac{\partial \bar{U}_i}{\partial x_j} = -\frac{1}{\rho}\frac{\partial \bar{p}}{\partial x_i} + \nu \frac{\partial^2 \bar{U}_i}{\partial x_j^2} - \frac{\partial \overline{u_i u_j}}{\partial x_j} + g_i \tag{2}$$

Where, $\bar{U}_i$ and $\bar{p}$ indicate the time averaged velocity and pressure, respectively. The term $\overline{u_i u_j}$ in Equation (2) refers to Reynolds stress tensor that is associated to turbulent viscosity, υ_t, based on the equation (3):

$$\overline{u_i u_j} = \nu_t \left(\frac{\partial u_i}{\partial x_j} + \frac{\partial u_j}{\partial x_i} \right). \tag{3}$$

To obtain the turbulent viscosity, both of $k\text{-}\omega$ and $k\text{-}\varepsilon$ methods can be used. As it was stated by ITTC Report [22] and De Luca et al.[23], there is no significant difference between k-ω and k-ε results for high speed planing hulls simulations. However, $k-\varepsilon$ method has been used in current work based on previous study [13].

To compute the boat motions, there are different methods which are available in Star-CCM+ such as rotation and translation, overset grid and morphing mesh approach. Based on previous studies such as Dashtimanesh et al. [14], morphing mesh is a robust approach which can support mesh movements in computational domain, especially around the boat hull. In fact, Star-CCM+ uses control points and their associated movements to generate an interpolation field throughout the computational region which can then be used to displace the actual vertices of the mesh. Each control point has an associated distance vector which specifies the displacement of the point within a single time step [24]. DFBI morphing is a variant of morphing motion which is used for computation of Dynamic Fluid Body Interaction (DFBI). Again, based on the previous experiences, DFBI mesh morphing can be utilized to control the computational procedure. Therefore, a system of equations is created related to *N* control vertices and specified displacements can be written as [24]:

$$d_i = \sum_{i=1}^{N} f_{b,j}(r_{ij})\lambda_j + \alpha, \tag{4}$$

where d_i' is displacement for each control vertex,*i*. Furthermore, $f_{b,j}(r_{ij})$ can be calculatedby equation (5) for any r_{ij}:

$$f_{b,j}\ \ r_{ij}\ \ = \sqrt{r_{ij}^2 + c_j^2}, \tag{5}$$

where c_j is a basic constant which is set to zero in Star-CCM+ and r_{ij} is calculated by equation (6):

$$r_{ij} = \left| x_i - x_j \right| \tag{6}$$

In this equation, x_i is the position of vertex $i.\lambda_i$ is also an expansion coefficient which can be written as follows:

$$\sum_{i=1}^{N} \lambda_i = 0 \tag{7}$$

It should be noted that α in equation (4) is a constant vector that is used to satisfy the additional constraints.

3. Modelling and Numerical Setup

At first, the tunneled planing hull model which is shown in Figure 1 is generated based on the principal dimensions in Table 1. It is observed that the initial hull model can be divided into three parts: a main hull and two side hulls.

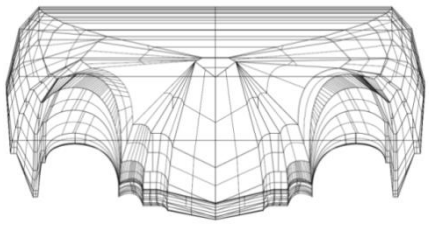

Fig. 1 Body plan of the tunneled hull model.

Table 1 Model dimensions [21].

Main feature	value
Length (m)	2.4
Moulded Breadth (m)	0.64
Average deadries angle (°)	13
Draft (m)	0.145
Initial trim angle (°)	3
Displacement (kg)	40
Length of center of gravity (m)	0.63

A right-handed coordinate system, xyz, is considered at the centerline in intersection between keel and transom. It is a global coordinate system which is fixed at the mentioned location. x and z coordinates are positive in forward and upward directions, successively. A local coordinate system is also defined at the boat center of gravity (CG). This coordinate system possesses all of the boat motions in different directions. As mentioned before, tunneled planing hull is only free to heave in η direction and pitch around ζ axis.

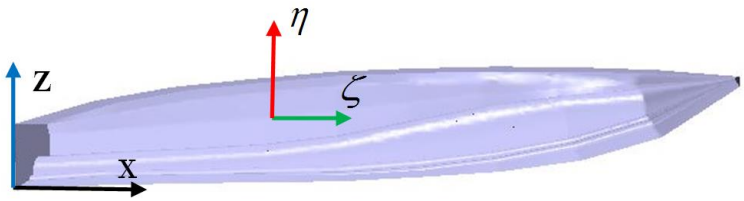

Fig. 2 Coordinate system definition.

3.1 Numerical setup

To simulate fluid flow around the tunneled planing hull, the computational domain is chosen in a way that the effects of boundaries reflections on numerical results are minimized. For this purpose, based on the previous experiences [14, 15], the length of computational domain is considered to be $6L_{OA}$ which ensures that there is no interaction between boat generated waves and outlet boundary. Furthermore, distance between boat and the bottom of computational domain is $3L_{OA}$ to satisfy deep water condition. Also, width of computational domain is assumed to be $1.5L_{OA}$ to minimize the flow reflection from the side boundaries. Figure 3 shows the computational domain and corresponding boundary conditions.

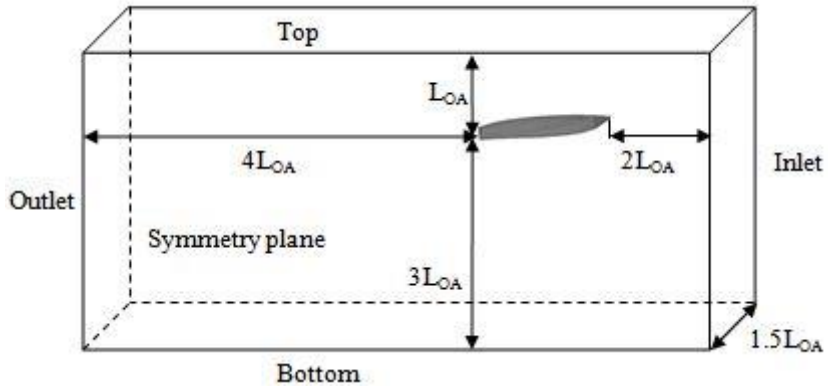

Fig. 3 Computational domain size and boundary conditions.

To solve the governing equations in considered computational domain, different boundary conditions are defined. The boundaries are introduced in the Figure 3 and corresponding boundary conditions are presented in table 2. The input, top and bottom boundaries are considered as velocity inlet which is air and water velocities, successively. Moreover, outlet boundary, located at left side of the domain, is prescribed as pressure outlet and two phases of fluid can exit from this boundary. The boat hull should be considered as a wall which means a no-slip boundary. Two remaining boundaries are investigated as symmetry plane. Symmetry plane condition is a zero slip boundary, which is utilized for mirror symmetry in hull geometry and flow pattern.

Table 2 Boundary conditions.

Boundary name	Boundary type	Volume fraction
Hull surface	wall	-
Domain inlet	Velocity inlet	Air and water
Domain outlet	Pressure outlet	Air and water
Domain top	Velocity inlet	Air
Domain bottom	Velocity inlet	water
Domain side	Symmetry plan	Air and water
Domain symmetry	Symmetry plan	Air and water

In addition to boundary conditions, it should be noted that the hydrostatic pressure in inlet and outlet boundaries can be obtained from the free surface location by specifying an atmospheric reference pressure in a point which is located above the free surface.

To generate the mesh over the computational domain, three different mesh structures have been employed. Surface mesh has been used in all regions of computational domain which have been smaller in hull surface. To presented wake profile in free surface behind the hull with a good accuracy, trimmer mesh has been defined in water surface as it is shown in Figure 4. Moreover, it can be seen that a prism layer mesh model is also used to generate the boundary layer mesh around the hull. In this study, wall y+ approach is used. It is very important to obtain a reasonable range of y^+ over the hull surface. Figure 5 shows the y^+ distributions on the hull bottom at highest Froude number 7.63.

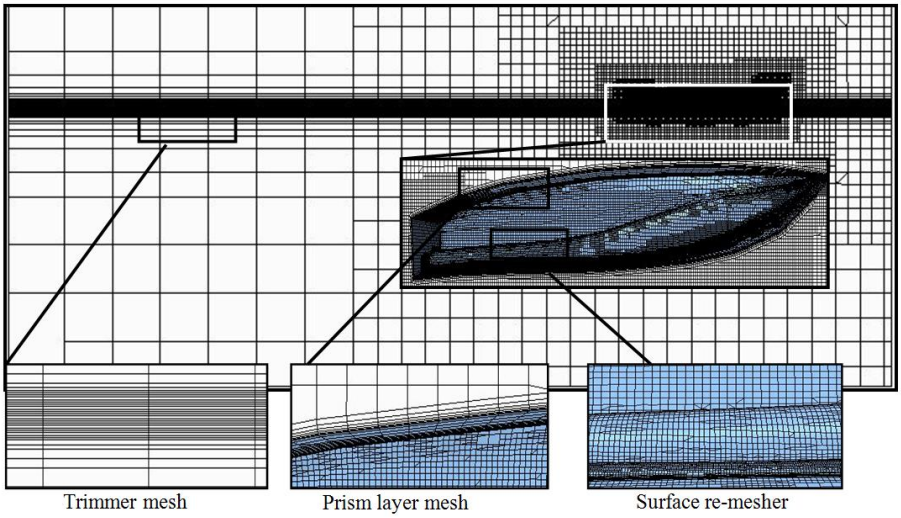

Fig. 4 Mesh structure on computational domain

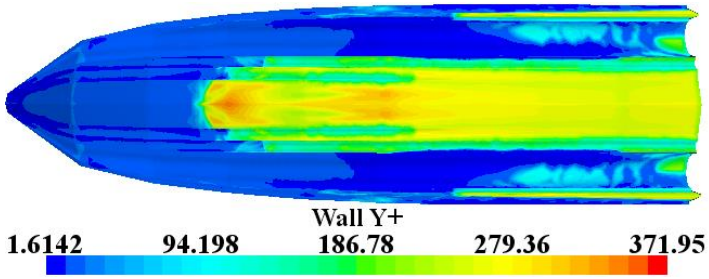

Fig. 5 Y^+ distribution on hull bottom at Fr = 7.63.

3.2 Grid independency

In numerical simulations, the appropriate choices for the time step and grid size ensure the robustness of the numerical computations because the stability and the solution convergence depend on the both time step and grid size, simultaneously. Therefore, the time step is set to be 0.0004s based on the previous experiences such as Dashimanesh et al. [14] to ensure that in the computational process, all the detailed fluid flow phenomena are captured. Moreover, four different cell numbers including 557400, 668622, 727009 and 807389 cells are utilized to ensure the independency of the obtained results from the cell numbers. In this regards, Figure 6 shows the obtained drag to lift ratio and dynamic trim in different cell numbers at Fr=7.63 which has been considered as maximum speed of tunneled planing hull in this study. According to Figure 6, there is only 0.5% difference between numerical solutions of 727009 and 807389 cells numbers in drag to lift ration, and 6.6% in trim angle. Therefore, it is clear that the numerical solution is mesh independent for the cell numbers more than 727009.Therefore, it will be reasonable to use 807389 cells for numerical computations in considered Froude numbers.

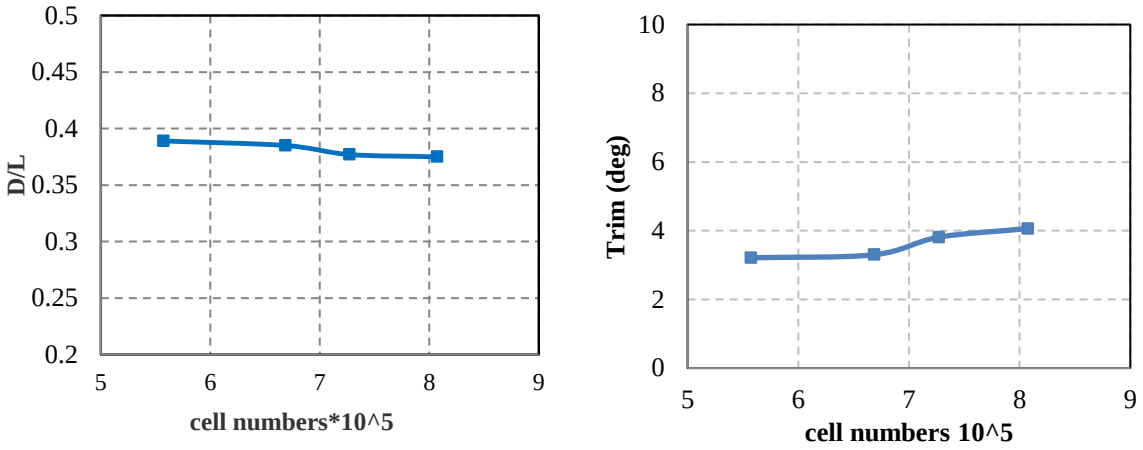

(a) Drag to lift ratio (b) Trim angle

Fig. 6 Non-dimension drag for various meshes in Fr = 7.63.

3.3 Comparison of numerical results with experimental data

To validate the numerical solution, obtained results are compared against experimental data which has been presented by Ma et al. [21]. They tested a model of tunneled planing hull in calm water and measured the trim angle, dynamic sinkage and drag. The studies of Ma et al. [21] are numerically reproduced to capture hydrodynamics of tunneled planing hull, more thoroughly. Figure 7 shows a comparison between numerical and experimental results for both drag to lift ratio (D/L) and trim angle. It is observed that the computed drag to lift ratio is in good agreement with experimental data. The Root Mean Square (RMS) error of numerical solution in prediction of drag to lift ratio is 7.17%.It is also obvious that the drag to lift ratio increases by increasing the Froude number.

In addition to D/L, Figure7 also shows a comparison between the computed and measured trim angles in different Froude numbers. Again, RMS error for trim angle prediction is calculated which is 17.145%. Based on the obtained results, it is clear that the presented numerical solution is relatively accurate in comparison with experimental data. Therefore, it can be implemented for detailed study of hydrodynamic characteristics of tunneled planing hulls. It should also be noted that authors have faced with lack of computational resources and tried to solve this issue by proper distribution of computational cells as discussed before.

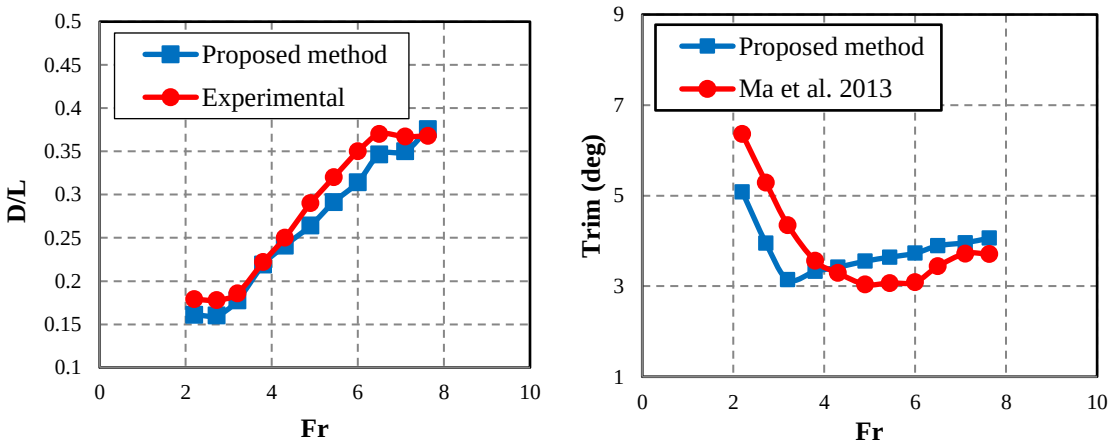

(a) Drag to lift ratio (b) Trim angle

Fig.7 Validation of numerical solution.

Shear and pressure drag contributions in total drag have been shown in Figure 8. It shows that, pressure drag is more than shear drag in Froude number 2.2, but shear drag increases as Froude number has been increased. Therefore, in higher Froude numbers, shear drag is dominant drag component.

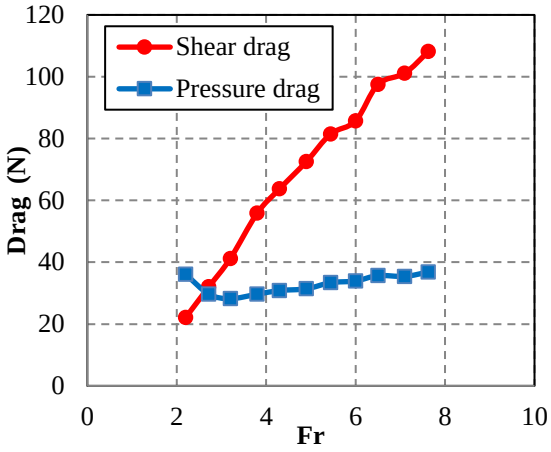

Fig. 8 Shear and pressure drag in different Froude numbers.

3.4 Wetted Surface and Flow path

Hull wetted surfaces are shown in Figure 9 for all investigated Froude numbers. It can be observed that, tunnel wetted surface is decreased by increasing the speed which causes air escaping from the tunnels and increasing the aerodynamic lift. The ventilation process starts from the spray rails and extends to chines. At Fr = 6.5, tunnel surface becomes dry and consequently, total drag reduces (Figure 9(i)). It is obviously clear that aerodynamic drag is less than hydrodynamic drag in tunnel surface. Figure 9 also shows that the chines have been designed in a way that remains connected to the water surface in all speeds to increase hull stability.

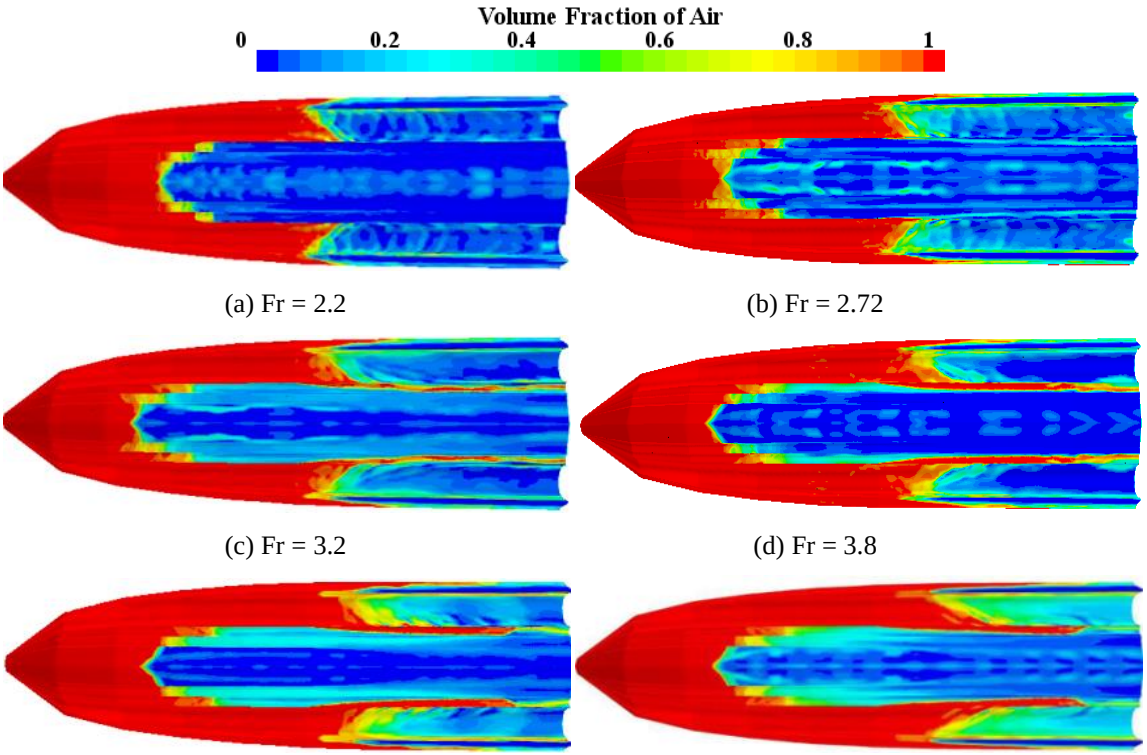

(a) Fr = 2.2 (b) Fr = 2.72

(c) Fr = 3.2 (d) Fr = 3.8

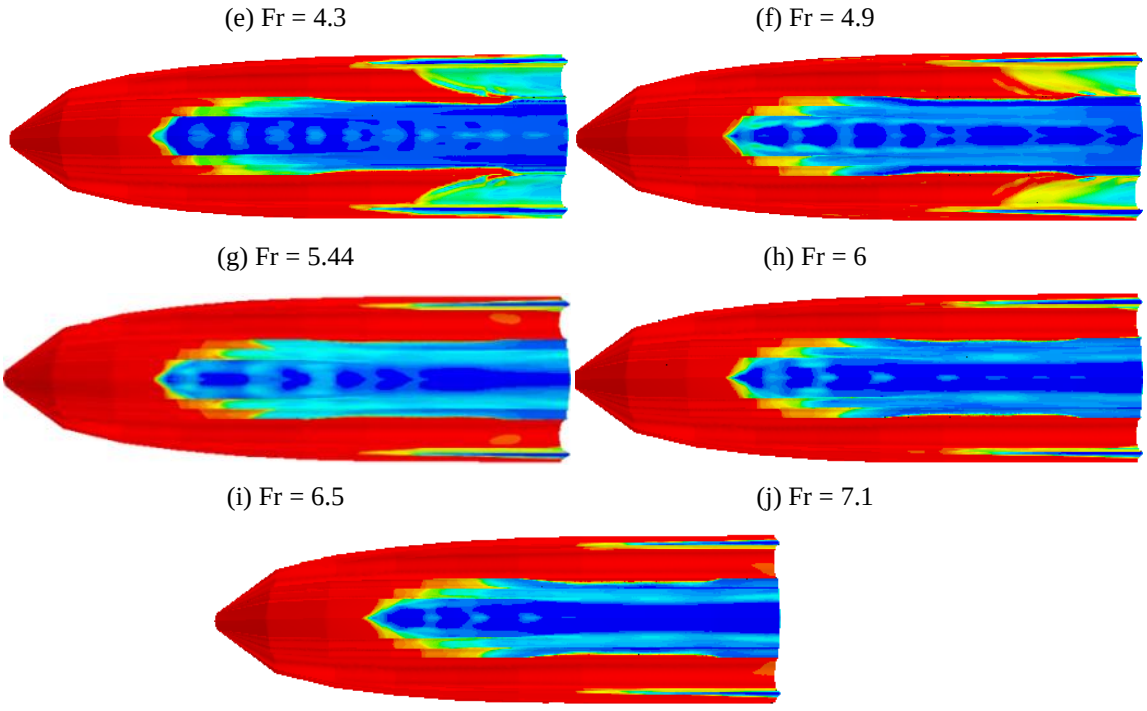

Fig. 9 Wetted surface in hull bottom.

Wetted length in keel and chine are also calculated for considered Froude numbers and presented in Table 3. It is observed that at Froude numbers less than 3.8, by increasing the velocity, the apex of stagnation line moves toward the bow and keel wetted length increases. However, the spray angle decreases and consequently, chine wetted length decreases which leads to wetted surface reduction. At Froude numbers higher than 3.8, trim angle increases by increasing the velocity and correspondingly, keel wetted length decreases. By reducing the keel wetted length, apex of stagnation line shifts toward the transom and spray angle decreases. Unlike the main hull, the trim angle interestingly, has no serious effect on wetted length of the lateral hulls.

Table 3 Wetted surface characteristics.

Fr	Trim angle (deg)	Keel wetted length (m)	Chine wetted length (m)	Spray angle (deg)	Tunnel wetted surface (m^2)	Total wetted surface ($m^{2)}$
2.2	5.08	1.46	0.92	63.4	0.29	1.16
2.72	3.98	1.49	0.83	62.31	0.29	0.98
3.2	3.143	1.57	0.82	56.91	0.26	0.94
3.8	3.328	1.58	0.78	54.9	0.25	0.90
4.3	3.417	1.553	0.75	51.9	0.24	0.83
4.9	3.553	1.55	0.72	45.36	0.19	0.78
5.44	3.64	1.513	0.7	40	0.14	0.73
6	3.728	1.51	0.59	33.31	0.10	0.60
6.5	3.892	1.41	0.51	31.31	0.01	0.53

7.1	3.96	1.5	0.48	29.64	0.008	0.53
7.63	4.061	1.5	0.42	17.83	0.006	0.50

Wetted surface at various Froude numbers is also presented in Table 3 that shows different parameters related to wetted characteristics for both main hull and tunnel surfaces. Generally, hull wetted are consists of wetted surfaces in hull bottom and tunnels. According to Table 3, at Froude numbers less than 6.5, hull wetted area decreases by increasing the speed which is mainly due to increasing the tunnel ventilation. Then for higher Froude numbers, tunnel have no contact with the water surface, so tunnel wetted area can be neglected. Also, variations of total wetted area at Froude numbers higher than 6.5 is negligible. It should be noted although wetted area decreases by increasing the velocity but keel wetted length increases till Fr = 3.8 and then its reduction starts.

Figure10 shows the free surface profile at different stations along the tunnel length. It is observed that by increasing the velocity, the chine for stations located in larger distance from the transom will remain dry. Moreover, it is clear that at higher Froude numbers, tunnel ventilation is increased and air region is extended to the transom. As it is shown in Figure10, tunnel surface is wetted before x/L=0.34 at Froude number 2.2. However, tunnel is ventilated in the same location at Froude numbers higher than 3.8. As it was shown in Figure10, tunnel ventilation started from spray rails which have been located at the internal side of the tunnel. By moving forward from middle stations toward the transom stern, air region is significantly decreases until tunnel surface is filled with water.

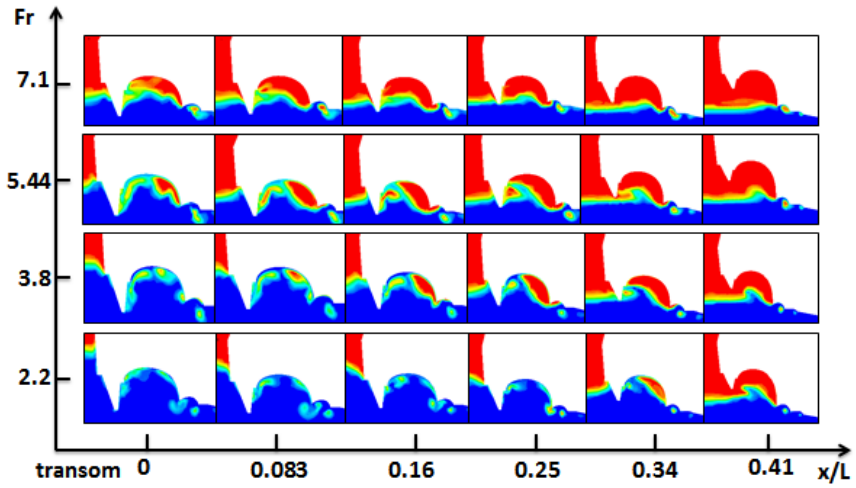

Fig.10 Volume fraction in tunnel for different cross sections at various Froude numbers.

Moreover, Figure 11 shows the distribution of skin friction coefficient over the hull bottom. It is clear that, the skin friction distribution depends on boat velocity and corresponding dynamic sinkage and trim angle. Maximum friction coefficient is occurred at both stagnation line and chine. It can also be seen that by increasing the Froude number, skin friction coefficient is increased over the hull wetted surface.

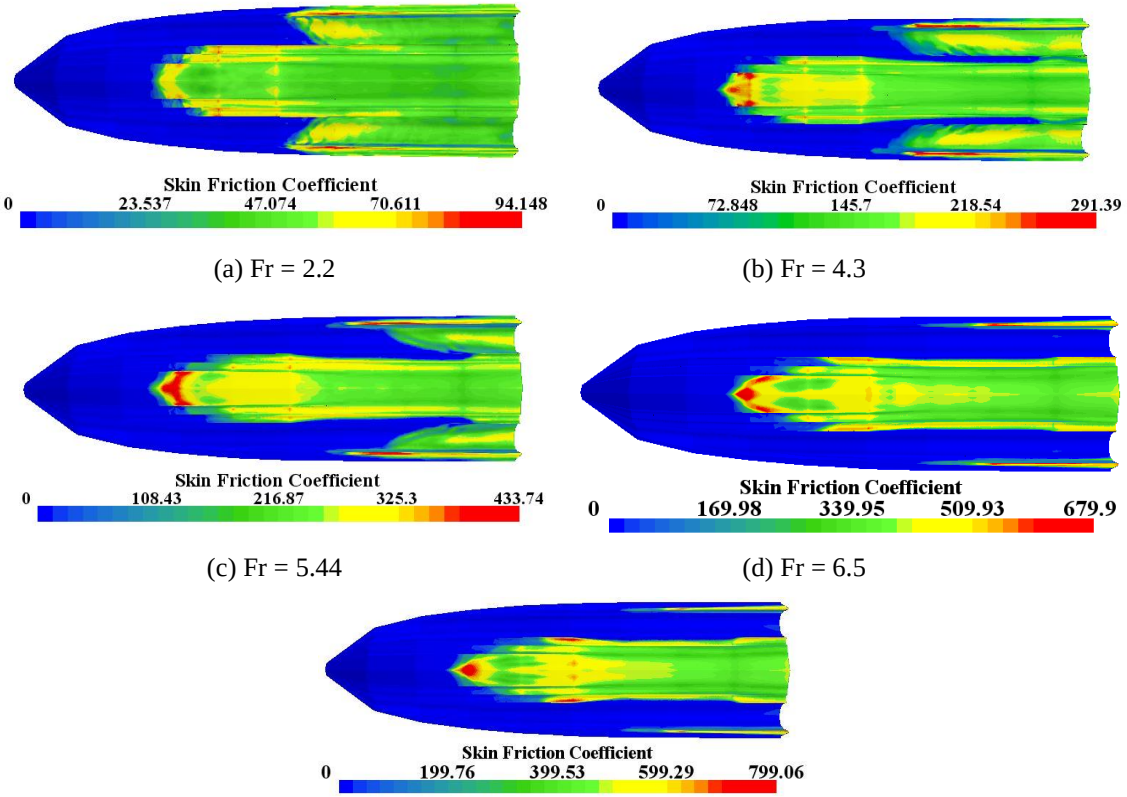

(a) Fr = 2.2 (b) Fr = 4.3

(c) Fr = 5.44 (d) Fr = 6.5

(e) Fr = 7.63

Fig. 11 Skin friction coefficient for various Froude numbers.

Skin friction coefficient over the planing length has been shown in Figure 12, to present more details of drag distribution. In this Figure, X is longitudinal distances from the transom and L_{OA} is tunneled hull length. It is clear that maximum friction drag occurs in stagnation point, which is located in $0.6L_{OA}$ distances from the transom, approximately. According to Figure 12, skin friction coefficient has a minimum value in $0.1L_{OA}$ distances from the transom and it increases as decreases distance from the transom.

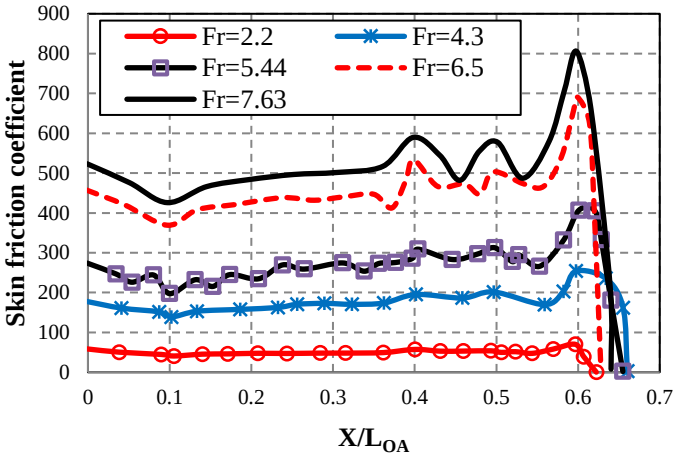

Fig. 12 Skin friction coefficient over the tunneled planing hull length.

As it was explained previously, both hydrodynamic and aerodynamic lifts may be generated by the tunnels. Therefore, it can be useful to explore details of fluid flow behavior in the tunnels. For this purpose, Figure 13 presents the streamline and flow pattern over the hull bottom at various Froude numbers. Air and water streamlines have been marked by use

of red and blue colures, respectively. Accordingly, a vortex flow of the air current is created in tunnels entrance, which leads to adverse pressure gradient in the hull surface and absorbing bow wave in the tunnels.

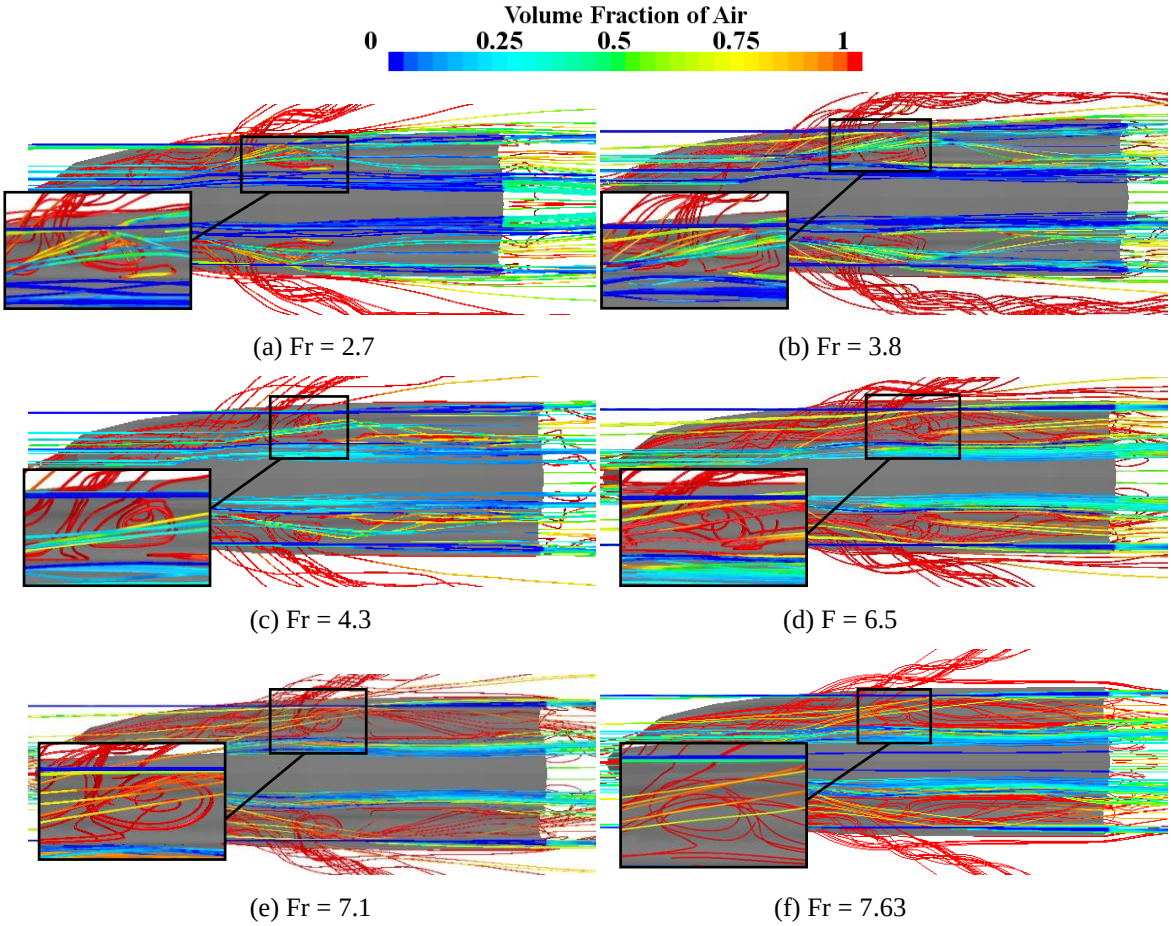

(a) Fr = 2.7 (b) Fr = 3.8

(c) Fr = 4.3 (d) F = 6.5

(e) Fr = 7.1 (f) Fr = 7.63

Fig.13 Streamline over the hull bottom at various Froude number.

The wake profile just behind the transom is also important to be investigated because of their effects on performance of tunneled planing hulls. The generated wake consists of both fluid and air particles. However, as SU et al. [6] have mentioned that, reduction of the stern wake is one of the hydrodynamic features of the channel type planing trimaran. Ghadimi et al. [25] and Dashtimanesh and Ghadimi [26] had observed that in the case of a prismatic planing hull, transom waves are rigorous mainly because of variation of pressure distribution over the hull near the transom and conversion of potential energy of water particle to kinetic energy. Moreover, Dashtimanesh and Ghadimi [27] have presented the effect of velocity in wave profile of stern transom and discussed that there is an energy transfer between fluid and hull which is increased by increasing hull velocity and therefore wave height behind the transom is amplified. Meanwhile, in the case of tunneled boats, the water particle energy has been damped in the tunnels. Generally, Figure 14 shows wave profile behind the hull in two longitudinal sections for considered Froude numbers. Transom is assumed to be located at zero on horizontal axis and water position in Z direction is shown on vertical axis. Free surface height in center line is shown in Figure 14(a). It is clear that, there is a hollow near the transom and as get away from the hull, water surface will back to initial draft. By increasing the velocity, hollow length has developed and wake height has decreased. In addition to centerline, wave pattern just behind the center of tunnel is illustrated in Figure 14(b).

According to this figure, again, hollow length increases by increasing the velocity but the flow behavior is different in comparison with that of boat centerline. In fact, it is observed that tunnel has damped the transom wave, effectively.

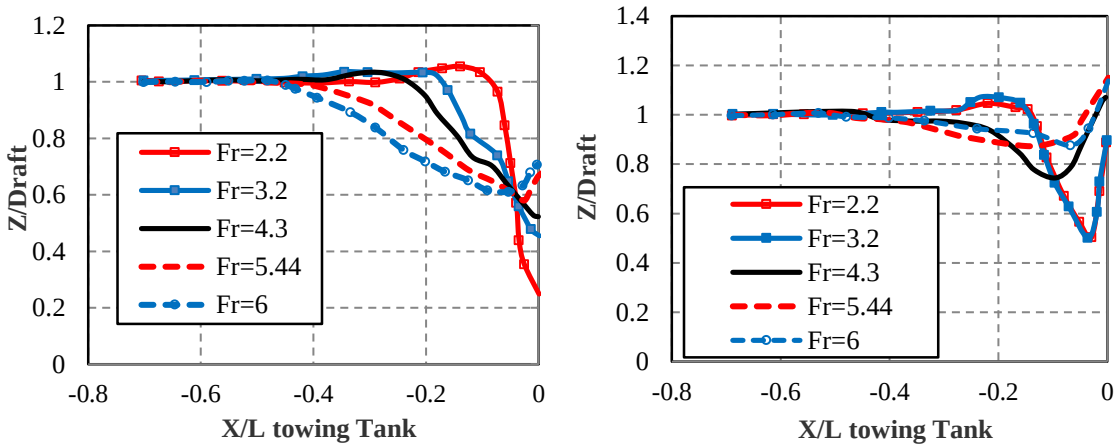

(a) y=0 (b) y=0.2

Fig. 14 Wake profile.

3.5 Pressure Distribution

Figure15 shows the pressure distribution over the hull bottom at various Froude numbers. It is observed that the maximum pressure occurs in stagnation line, in the middle of tunnel surface and increases by increasing the Froude number. Acting pressure over the hull bottom contains some positive and negative values. Instantly behind the stagnation line, pressure has reduced to a negative value. However, in the pressure regions at the bow and near the transom, pressure values are positive. This behavior is completely similar to what has been reported by Su et al. [6] and Jiang et al. [10] for tunneled planing hulls.

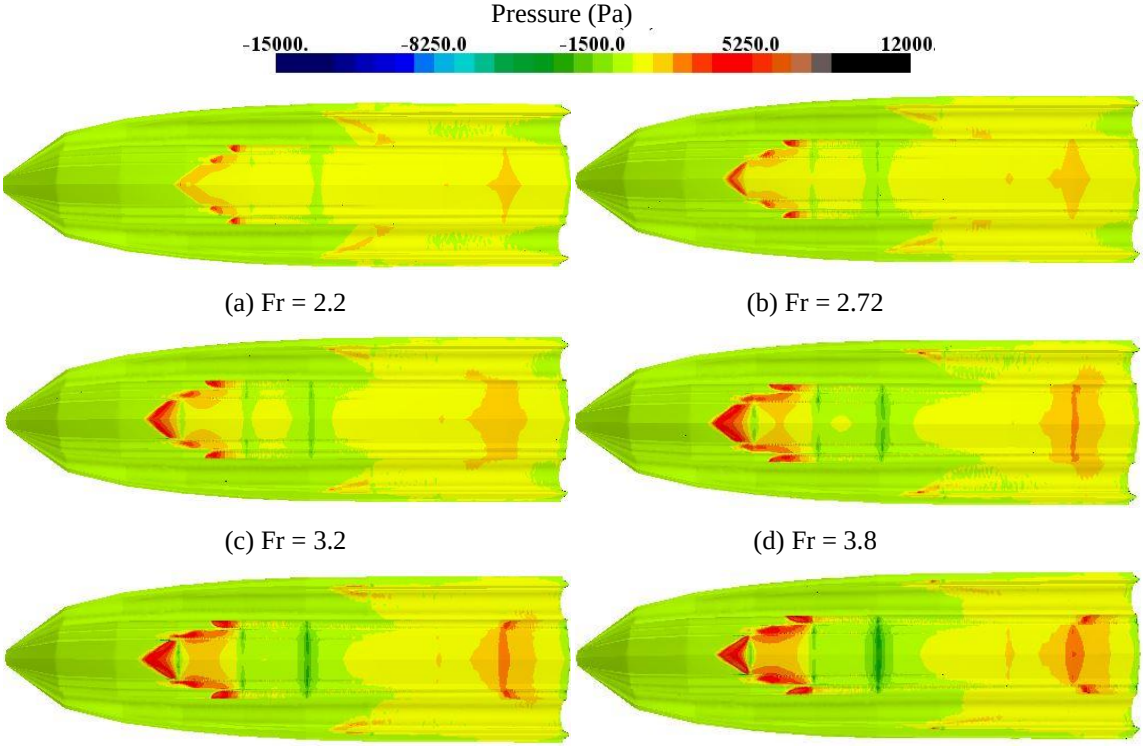

(a) Fr = 2.2 (b) Fr = 2.72

(c) Fr = 3.2 (d) Fr = 3.8

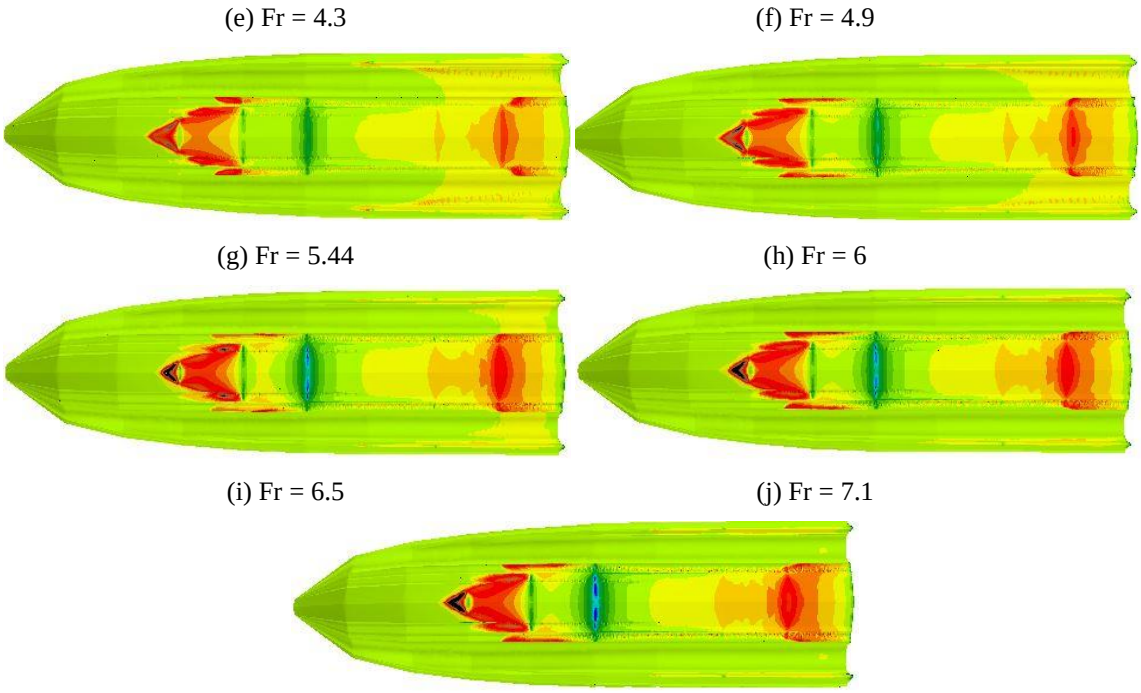

(e) Fr = 4.3 (f) Fr = 4.9

(g) Fr = 5.44 (h) Fr = 6

(i) Fr = 6.5 (j) Fr = 7.1

(k) Fr = 7.63

Fig. 15 Pressure distributions in different Froude numbers.

To analyze the hydrodynamic pressure on the bottom of tunneled hulls more thoroughly, longitudinal pressure coefficients acting on the keel are presented for various Froude numbers in Figure16, where x is the distance from the transom. It is clear that, negative pressure on hull bottom occurs at $X/L_{OA}=0.4$ from the transom for all Froude numbers. Negative pressure on hull bottom is similar to the ventilated region behind the steps in stepped planing hulls [14]. Therefore, it can be concluded that adding a step near the $X/L_{OA}=0.4$can lead to increasing the hull resistant for considered hull which has also been shown by Ma et al. [21], experimentally.

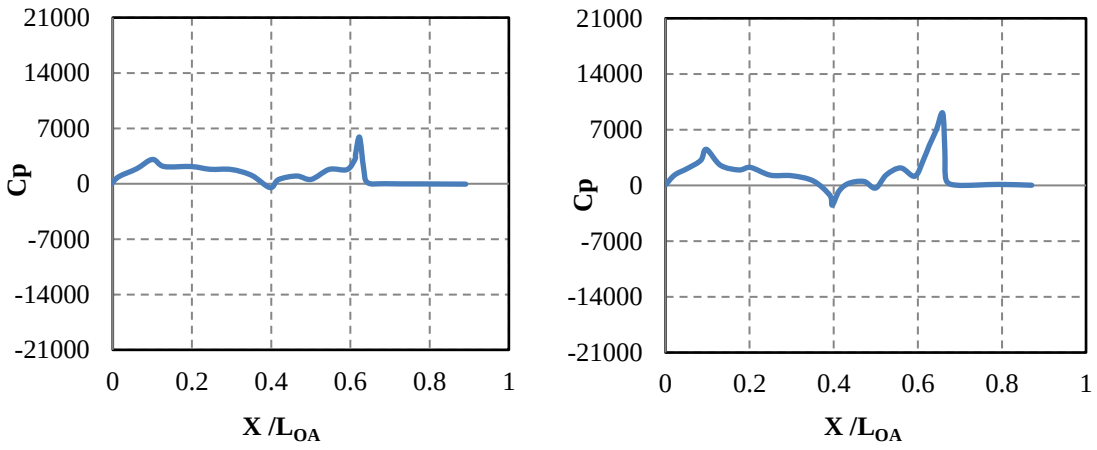

(a) Fr = 2.72 (b) Fr = 5.44

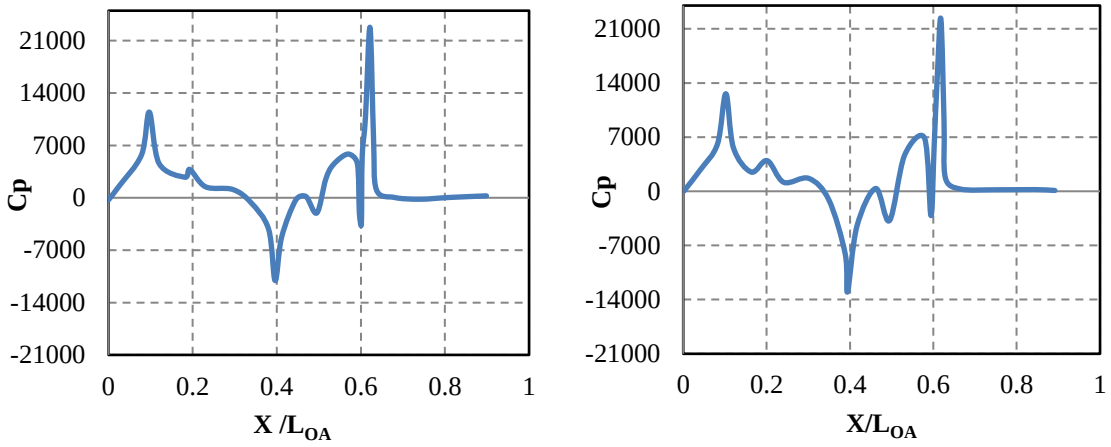

(c) Fr = 7.1 (d) Fr = 7.63

Fig. 16 Pressure coefficient in boat's centreline.

Figure 17 presents hydrodynamic pressure distribution around the tunnel in different transverse sections at considered Froude numbers. According to pressure contour, there is a zero hydrodynamic pressure zone in tunnel at all Froude numbers which is increased by increasing Froude number. Therefore, it can be stated, this vacuum region has been occurred due to tunnel ventilation, which has been presented in section 4.3. Moreover, Figure 17 also shows that in planing regime, station 0.2 has maximum hydrodynamic pressure of tunnel and at this position, hydrodynamic pressure become increased at spray rail.

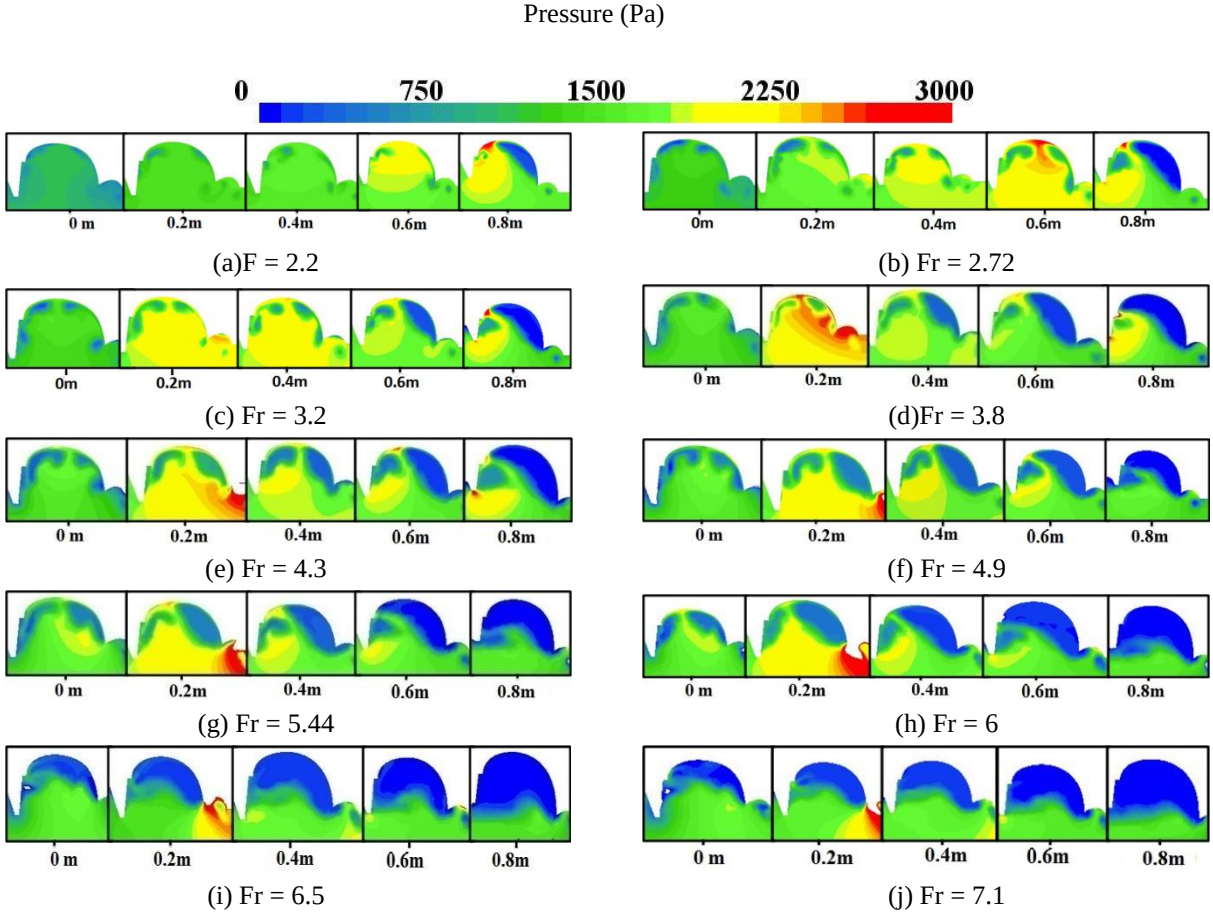

(a)F = 2.2 (b) Fr = 2.72

(c) Fr = 3.2 (d)Fr = 3.8

(e) Fr = 4.3 (f) Fr = 4.9

(g) Fr = 5.44 (h) Fr = 6

(i) Fr = 6.5 (j) Fr = 7.1

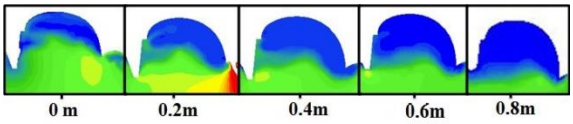

(k) Fr = 7.63

Fig. 17 Hydrodynamic pressure around the tunnel in different Froude numbers.

One of the other factors that are very important is lift to drag ratio, which can be used to determine the hull efficiency. Moreover, to analyze the tunnel effect for lift generation, tunnel lift to total lift ratio is presented in Figure 18(a)at different Froude numbers. It is observed that this ratio reduces suddenly at Fr=6.5, because the interference effects between tunnel and water surface decreases significantly. In order to introduce the tunnel efficiency, lift to drag ratio in tunnel is also presented in Figure 1(b) as a fraction of total lift to drag ratio. At Froude numbers less than 6, tunnel efficiency is increased by constant rate as the velocity increases. At higher Froude numbers, tunnel effect on hull efficiency is increased, rapidly. Because in these Froude numbers, tunnel surface has been ventilated totally and tunnel drag is very small. Therefore, denominator of equation (17) is reduced and tunnel efficiency has been increased:

$$\eta=\frac{\text{tunnel Lift/tunnel Drag}}{\text{Total Lift/Total Drag}} \tag{17}$$

Then, it can be stated that for Froude numbers higher than 6, tunnel is more efficient.

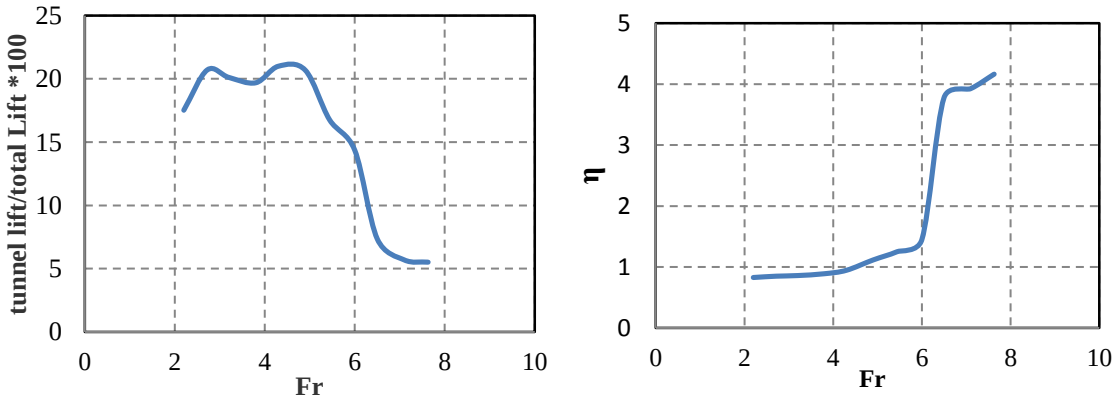

(a) Tunnel lift (b) Tunnel efficiency

Fig. 18 Lift Force.

As it was shown in Figure 9 tunnel surface have been ventilated totally in Froude numbers higher than 6. Therefore, using tunneled configuration for design speed higher that 6 is more useful in drag reductions (Figure18). Moreover, showing pressure distribution around hull shown that there is a negative pressure region in x/l=0.4 which have a high skin friction drag.

4. Conclusions

In this study, a tunneled planning hull with two degrees of freedom in heave and pitch directions was simulated in Star-CCM+ and some of hydrodynamic characteristic which have been avoided by previous researchers were presented in details. These parameters help to design an appropriate tunneled hull due to tunnel efficiency in design speeds. In this way, two phases of fluid around the hull were defined by using VOF method in conjunction with $k-\varepsilon$ turbulence model. Hull resistance as well as running attitude of the boat was validated against the experimental data. Obtained results show that shear drag is the main part of total drag of

tunneled hull. Therefore, skin friction distribution over the hull surface was studied in details. It shows that, maximum skin drag was occurred at the stagnation line and transom which was increased by increasing the hull speed. Also, minimum skin drag was occurred in some distances from the transom. Moreover, stagnation line with maximum friction drag depends on hull speed and trim angle. Therefore, it was shifted forward by increasing the speed up to Fr = 3.8, due to trim angle variation. However, for higher Froude numbers, stagnation line was move backward by increasing the Froude number. Wetted surface area and its contours were also provided for considered Froude numbers. It was seen that tunnels have separated from the water surface in Froude number higher than 6 and wetted area decreases. In these speed regimes, tunnel has a good effect on planing hull performance. Furthermore, tunnel ventilation was shown for various speeds in different cross sections. Then, it was found that tunnel ventilation has started from the spray rails and extended to the chines by increasing the speed. Moreover, streamlines around the hull showed that vortex air flow has occurred in the tunnel where air flow leaves the tunnel from the chine. Afterwards, wake profile was presented for investigated Froude numbers in two longitudinal sections behind the transom. In addition, pressure distribution and its contour were shown in hull bottom. It is shown that, there is a negative pressure zone in hull bottom at same length for all considered Froude numbers. Moreover, pressure distributions in tunnel were presented in different distances from the transom. Finally, tunnel lift percentage and tunnel efficiency were investigated and obtained results shows that tunnel have good advantage for drag reduction of high speed craft in Froude numbers higher than 6. For lower Froude number using tunnel in hull form is no logistical.

In future studies, more hydrodynamic details of tunneled planing hulls will be investigated. Specifically, behavior of tunneled boats in sea waves will be simulated and discussed. Moreover, it is aimed to consider interaction between tunnels and surface piercing propeller.

REFERENCES

[1] Blount, Donald L.: "Design of propeller tunnels for high-speed craft", Proceedings of 4th FAST Conference, 1997.

[2] Millward, A.: "The effect of channel width and depth on the resistance of a high speed hull", International shipbuilding progress 51, No. 4, 2004.

[3] Subramanian, V. Anantha, P. V. V. Subramanyam, and N. Sulficker Ali.: "Pressure and drag influences due to tunnels in high-speed planing craft", International shipbuilding progress54, no. 1, 2007.

[4] Campbell, L.F.: "Entrapment tunnel monohull optimized waterjet and high payload", U.S. Patent No. 7,418,915. 2 Sep. 2008.

[5] Zou, J., Wang, Q.X., Shi, S.Z., Zhou, J.: "The Brief Introduction of High-Speed Trimaran Planing Hull and the Preliminary Study of the Longitudinal Stability", In Applied Mechanics and Materials (Vol. 117, pp. 559-564). Trans Tech Publications, 2012. https://doi.org/10.4028/www.scientific.net/AMM.117-119.559

[6] SU Y.M., Shuo W.A.N.G., SHEN H.L., Xin D.U.: "Numerical and experimental analyses of hydrodynamic performance of a channel type planing trimaran", Journal of Hydrodynamics, Ser. B, 2014. https://doi.org/10.1016/S1001-6058(14)60062-7

[7] SU Y.M, Shuo W.A.N.G., SHEN H.L.: "Experimental study on resistance performance of channel type planing trimaran model", Journal of Harbin Engineering University, VOL.34. No.7, 2013.

[8] Yousefi R., Shafaghat R., Shakeri M.: "High-speed planing hull drag reduction using tunnels", Ocean engineering, 84, 2014. https://doi.org/10.1016/j.oceaneng.2014.03.033

[9] Ghassabzadeh M. and Ghassemi H.: "Numerical hydrodynamic of multihull tunnel vessel", Open Journal of Fluid Dynamics, 2013. https://doi.org/10.4236/ojfd.2013.33025

[10] Jiang Y., Sun H., Zou J., Hu A. and Yang, J.,: "Experimental and numerical investigations on hydrodynamic and aerodynamic characteristics of the tunnel of planing trimaran", Applied Ocean Research, 63, 2017. https://doi.org/10.1016/j.apor.2016.12.009

[11] KazemiMoghadam H., Shafaghat R., Yousefi R.: "Numerical investigation of the tunnel aperture on drag reduction in a high-speed tunneled planing hull", Journal of the Brazilian Society of Mechanical Sciences and Engineering, 37(6), 2015. https://doi.org/10.1007/s40430-015-0431-4

[12] KazemiMoghadam H., Shafaghat R.: "Numerical investigation on the effect of tunnel height on drag reduction in a high speed trimaran", International journal of maritime technology, Vol.5, 2016.

[13] Ghadimi, P., Mirhosseini, S.H., Dashtimanesh, A., Amini, M.: "RANS Simulation of Dynamic Trim and Sinkage of a Planing Hull", Applied Mathematics, 1(1), 2013. https://doi.org/10.1155/2013/868252

[14] Dashtimanesh A., Esfandiari A., Mancini, S.: "Performance Prediction of Two-Stepped Planing Hulls Using Morphing Mesh Approach". Journal of Ship Production and Design, 2018. https://doi.org/10.5957/JSPD.160046

[15] Bilandi, R. N., Dashtimanesh, A., Tavakoli, S.:"Hydrodynamic study of heeled double-stepped planing hulls using CFD and 2D+ T method", Ocean Engineering, 196, 106813, 2020. https://doi.org/10.1016/j.oceaneng.2019.106813

[16] Dicaterino, F., Bilandi, R. N., Mancini, S., Dashtimanesh, A., and Carlini, M. D.: "A Numerical Way for a Stepped Planing Hull Design and Optimization", In Technology and Science for the Ships of the Future: Proceedings of NAV 2018: 19th International Conference on Ship & Maritime Research (p. 220). IOS Press, 2018.

[17] Dashtimanesh, A., Roshan, F., Tavakoli, S., Kohansal, A., and Barmala, B.:"Effects of step configuration on hydrodynamic performance of one-and doubled-stepped planing flat plates: A numerical simulation", Proceedings of the Institution of Mechanical Engineers, Part M: Journal of Engineering for the Maritime Environment, 1475090219851917, 2019. https://doi.org/10.1177/1475090219851917

[18] Ghadimi, P., Dashtimanesh, A., Farsi, M., and Najafi, S.: " Investigation of free surface flow generated by a planing flat plate using smoothed particle hydrodynamics method and FLOW3D simulations", Proceedings of the Institution of Mechanical Engineers, Part M: Journal of Engineering for the Maritime Environment, 227(2), 125-135, 2013. https://doi.org/10.1177/1475090212465235

[19] Subramanian V.A., Subramanyam P.V.V.: "Effect of tunnel on the resistance of high-speed planing craft", Journal of Naval Architecture and Marine Engineering, 2(1), 2005. https://doi.org/10.3329/jname.v2i1.2025

[20] Jiang Y., Sun H., Zou J., Hu A., Yang J.: "Analysis of tunnel hydrodynamic characteristics for planing trimaran by model tests and numerical simulations", Ocean Engineering, 113, 2016. https://doi.org/10.1016/j.oceaneng.2015.12.038

[21] Ma W., Sun H., Zou J., Yang H.: "Test research on the resistance performance of high-speed trimaran planing hull", Polish maritime research, 20(4), 2013. https://doi.org/10.2478/pomr-2013-0040

[22] ITTC, "Specialist committee on CFD in marine hydrodynamics—27thITTC", 2014.

[23] De Luca, F., Mancini, S., Miranda, S., Pensa, C.: "An extended verification and validation study of CFD simulations for planing hulls", Journal Ship Research 60 (2), 2016. https://doi.org/10.5957/JOSR.60.2.160010

[24] STARCCM+ Inc.: "Fluent 6.3 User's Guide", 2006F.

[25] Ghadimi, P., Dashtimanesh, A., and Chekab, M. A. F.: "Introducing a new flap form to reduce the transom waves using a 3-D numerical analysis", International Journal of Computational Science and Engineering, 12(4), 265-275, 2016. https://doi.org/10.1504/IJCSE.2016.076934

[26] Dashtimanesh, A. and Ghadimi, P.: "A three-dimensional SPH model for detailed study of free surface deformation, just behind a rectangular planing hull", Journal of the Brazilian Society of Mechanical Sciences and Engineering, 35(4), 2013. https://doi.org/10.1007/s40430-013-0035-9

[27] Dashtimanesh, A., & Ghadimi, P.:"SPS turbulent modeling of high speed transom stern flow", Brodogradnja: Teorija i praksa brodogradnje i pomorske tehnike, 65(1), 1-16, 2014. https://doi.org/10.14419/ijpr.v1i1.726

Submitted: 16.11.2018.
Accepted: 10.01.2020.

Fatemeh Roshan, Department of Marine Technology, Persian Gulf University
Abbas Dashtimanesh (*corresponding author), Estonian Maritime Academy, Tallinn University of Technology, Department of Marine Technology, Persian Gulf University
abbas.dashtimanesh@taltech.ee
Rasul Niazmand Bilandi, Department of Marine Technology, Persian Gulf University